JOURNAL OF Materials CHEMISTRY

Reversible intercalation of volatile amines into stacks of soluble phthalocyanines

Christopher Fietzek,*[a] Michael Seiler,[d] Bernd Görlach,[b] Peter Schütz,[a] Udo Weimar,[a] Michael Hanack,[b] Christiane Ziegler[c] and Helmut Bertagnolli[d]

[a]*Institute of Physical and Theoretical Chemistry, University of Tübingen, Auf der Morgenstelle 8, 72076 Tübingen, Germany. Tel: ++49 7071 29 78766; Fax: ++49 7071 29 5960; E-mail: christopher@.fietzek.de*
[b]*Institute of Organic Chemistry, University of Tübingen, Auf der Morgenstelle 18, 72076 Tübingen, Germany*
[c]*Institute of Physics, University of Kaiserslautern, Erwin Schrödinger Str. 56, 67663 Kaiserslautern, Germany*
[d]*Institute of Physical Chemistry, University of Stuttgart, Pfaffenwaldring 55, 70569 Stuttgart, Germany*

Received 21st January 2002, Accepted 18th April 2002
First published as an Advance Article on the web 20th June 2002

Different alkyl amines were intercalated into stacks of tetraalkenylphthalocyaninatozinc by exposing the solids to amine vapor. Since the intercalation is reversible, quantitative and kinetic aspects of the sorption were investigated using quartz crystal microbalances (QCMs) and thermal desorption mass spectrometry (TDS). Two different types of sorption were found and these were interpreted as interaction with aliphatic sidechains and preferential intercalation. At higher vapor concentration most of the interstitial spaces are occupied, suggesting a 1 : 1 host–guest stoichiometry. Structure elucidation of an intercalated *n*-butylamine was carried out by EXAFS transmission measurements. Intercalation was found to take place while maintaining the columnar arrangement and without significant expansion of the spacing. Additional QCM measurements revealed less favorable sorption of sterically demanding amines which can be explained by morphological discrimination.

Introduction

Many applications including process control, quality management and warning systems require the fast and cheap detection of specific gaseous analytes. Particularly in the case of volatile organic compounds (VOCs), among them volatile amines, there still exists a lack of appropriate sensors or sensor systems. The up-to-date approach to monitor VOCs by sensors is to use sensor arrays, *e.g.* mass sensitive devices, coated with films of polymers of poor selectivity and subsequently to distinguish between different analytes by using a data evaluation step.[1–4] A key problem of this solution is the redundant information caused by an increased number of sensors, the crucial data evaluation thus becoming less precise.[5]

In order to achieve selective gas sensors the most elegant solution, although also the most difficult, is to synthesize new highly selective materials. In the optimum case such sensors could be used as stand-alone devices. There are two types of selective criteria. On the one hand there is functionality, such as Lewis acidity in metal-containing materials,[6–10] ionic structures[11] or extremely active H-bonds.[12] However, on the other hand chemical sensor selectivity can be achieved using morphological effects, such as inclusion in cage compounds (among them crown ethers, cyclodextrins and paracyclophanes),[9,13,14] molecular imprinted materials,[15] microporous materials[16] or by the disarrangement of liquid crystals.[17]

For gas sensing applications phthalocyanines (PcMs) and the related class of porphyrins are well known for their good performance and their diverse chemical structure. In particular the facility to replace the central metal atom in the center of the molecule has a strong impact on the sensing properties. For example, in the case of zinc high affinities for amines were reported for porphyrins,[10,18,19] and phthalocyanines.[20] For nickel as the central atom high affinities for planar aromatic compounds were reported.[6] In the latter case the additional effect of π–π-interactions is discussed.[21]

The structures of solid phthalocyanines bearing long alkyl sidechains at the periphery of the molecule can be very different. At elevated temperatures some of these molecules assemble in liquid crystal structures, *e.g.* discotic mesophases.[22] At room temperature no macroscopic crystals are usually observed, but crystalline behaviour over a range of a few hundred nanometres is found.[6] These compounds can therefore be considered to be nanocrystalline, the intermolecular arrangement thereby being strongly influenced by the position and number of the substituents. Four different arrangements of heavily substituted PcMs are proposed by UV/VIS spectroscopy:[23] Substitution at all of the 16 available positions results in isolated molecules. If non-peripheral substituents are used, an edge to edge arrangement can be observed. Peripherally substituted PcMs tend to crystallize in columnar or herringbone-like arrangements, whereas longer sidechains favor a columnar arrangement with maximum spacing between adjacent two molecular planes.[24] The columnar arrangement is of special interest for chemical sensing because potential recognition sites are located inside the columns and so target compounds could therefore be selected by morphological properties: a docking inside the phthalocyanine stacks suggests an exclusion of large molecules, *e.g.* sterically demanding amines. This mechanism could be the reason for their good separation ability in distinguishing from simple amines in gas chromatography, when packed columns of unsubstituted zinc phthalocyanine adsorbed on graphitized carbon black are used.[20]

For the investigation of kinetic aspects and a potential use in sensor applications or capillary gas chromatography, a high mobility of VOCs inside the coatings is required. In general mobility in the solid phase is enhanced by introducing rotating molecular segments, as *e.g.* realized with polysiloxanes or

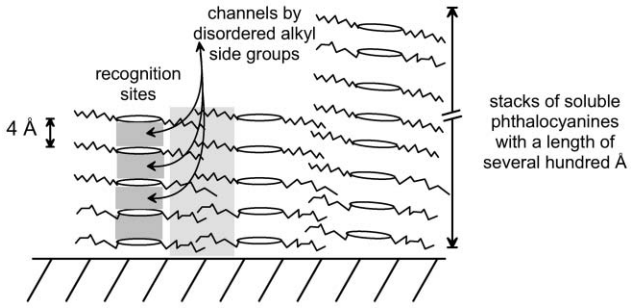

Fig. 1 Schematic drawing of the sorption process and the supposed structure of the phthalocyanine stacks.[6,24]

polymers bearing alkyl residues. With regard to the PcMs investigated, linear alkyl chains were chosen to favor fast absorption and desorption processes. Channels for the analytes are built and give access to the coordination centers throughout the film (*cf.* Fig. 1).

Thermal desorption mass spectrometry (TDS) and quartz crystal microbalance (QCM) experiments were performed in order to prove both bulk interaction and morphological discrimination. Based on the findings of Sauerbrey[27] mass sensitive devices like the QCMs are especially suited to measuring the mass uptake of volatile organic compounds (VOCs).[28] This is because these gases possess high molecular masses compared with permanent gases (*i.e.* gases with a critical temperature below room temperature).

The quantitative description of the QCM signals for coatings with sorption sites of different affinities has been described by Bodenhöfer *et al.*[29] If an interaction with the sensitive coatings is mainly nonspecific and is not limited in number or location, the signal is proportional to the gas concentration c. The behavior of the sensor can be described by Henry's law:

$$\Delta f_{\text{nonpreferential}} = K_{\text{Henry}} c \tag{1}$$

where $\Delta f_{\text{nonpreferential}}$ denotes the frequency decrease upon gas uptake and K_{Henry} is a constant.

For coatings with defined recognition sites (in this work the Lewis coordination to the metal center) an extended model based on superposition of preferential and non-preferential sorption was established.[13,30] In this model the frequency decrease $\Delta f_{\text{preferential}}$ due to preferential sorption is described by a Langmuir type equation:

$$\Delta f_{\text{preferential}} = A \frac{K_{\text{Langmuir}} c}{1 + K_{\text{Langmuir}} c} \tag{2}$$

K_{Langmuir} is a constant which determines the initial slope of the Langmuir curve. From a kinetic point of view K_{Langmuir} can be interpreted as the ratio of the kinetic constants of the adsorption and desorption process from a recognition site. The constant A corresponds to the sensor signal at complete coverage of all preferential sorption sites. The overall sensor response is given by

$$\Delta f_{\text{sum}} = \Delta f_{\text{preferential}} + \Delta f_{\text{nonpreferential}} \tag{3}$$

Since the QCM sensors allow exact determination of both the number of PcM molecules and the specifically adsorbed gaseous analytes, it is possible to determine the stoichiometric relationship between host and guest molecule. For any coating which has preferential sorption sites, the stoichiometry x of the host–guest complex can be determined using the following equation:

$$x_{\text{stoichiometric}} = \frac{A M_{\text{PcM}}}{\Delta f_{\text{PcM}} M_{\text{Analyte}}} \tag{4}$$

Δf_{PcM} denotes the frequency obtained with the coating procedure and A the amount of specifically absorbed analyte. M denotes the molecular masses of the compounds [M(*n*-butylamine) = 73.1 g mol^{-1}, M(*n*-propylamine) = 59.1 g mol^{-1}].

Regarding the structure elucidation of the complexes investigated, in particular of the host–guest complex in this paper, a zinc containing phthalocyanine has been studied as an amorphous solid by transmission extended X-ray absorption fine structure (EXAFS) spectroscopy. EXAFS spectroscopy has been considered to be a powerful technique for determining the local atomic environment of a specific atom independent of the state of the sample. EXAFS analysis provides information on the bond distance, the coordination number, the "Debye–Waller" factor and the nature of the scattering atoms surrounding an excited atom.[25,26]

2 Experimental

2.1 Chemicals

The compounds investigated are 2,9,16,23-tetrakis(hex-5-enyloxy)phthalocyanine and the corresponding zinc containing phthalocyaninato complex. The sidechain length of the zinc compounds was varied using three, six or eleven carbon units. The structures are shown in Fig. 2. The compounds were prepared according to standard procedures and checked for purity by ^{1}H-NMR. Details of the preparation can be found in ref. 31.

With reference to coatings with nonspecific VOC binding properties the polymer polyetherurethane (PEUT, Thermedics Inc., Woburn, MA) was chosen (Fig. 3).

2.2 Measuring procedure

Quartz crystal microbalance measurements. Discrete quartz microbalances operating at a thickness shear-mode resonance were used as transducers. The sensors consisted of piezoelectric quartz crystals (AT-cut) with gold electrodes operating at a fundamental frequency of f_o = 30 MHz (KVG, Quartz Crystal Technology GmbH, Germany). Each crystal was driven by a home-made oscillator circuit. The QCM output was monitored using a Hewlett Packard 5334B frequency counter and was recorded every 30 s with 0.1 Hz resolution. Simultaneous measurements from up to 16 sensors were made using a scanner controlled by a PCL 726 interface card (Labtech, Wilmington, MA) in an IBM compatible PC-AT. The sensors were prepared

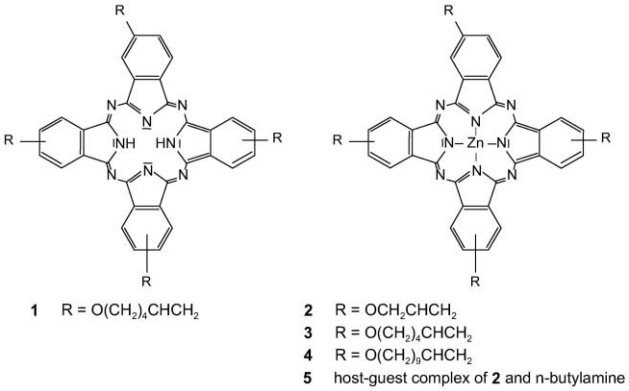

Fig. 2 Structural formulae of the 2,9,16,23-tetrakis(hex-5-enyloxy)-phthalocyanine and the tetrakis(alkenyloxy)phthalocyaninatozinc complexes.

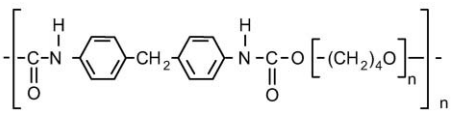

Fig. 3 Reference polymer polyetherurethane (PEUT).

by airbrush coating. Each substance was dissolved in dichloromethane (approx. 3 mg ml^{-1}) and sprayed onto the cleaned surfaces of the QCM sensors using synthetic air as the carrier gas. During the coating procedure the frequency change of the resonators was monitored. The process was stopped as soon as a shift of 40 kHz was reached on each side. An overall frequency shift of 80 kHz corresponds to a layer thickness of at least 160 nm per side, assuming a homogeneous layer of PcM and a density of 1.2 g mol^{-1}.[32] The test gases were generated by controlled evaporation at low temperatures and dilution with synthetic air using a gas mixing station.[33] The total gas flow rate (analyte gas and synthetic air) to the sensors was adjusted to 200 ml min^{-1}. The measurement chamber had a volume of 2 ml. The temperature of the chamber was adjusted between 298 and 318 K using a circulation cooling system (Julabo, Seelbach, Germany). Signals were determined from the frequency difference Δf between gas exposure and purging with analyte-free air.

Thermal desorption mass spectrometry (TDS). For thermal desorption mass spectrometry (TDS) stainless steel foil was used as the substrate. It was cleaned in acetone and in an oxygen plasma. Then an amount of the pure **3** was prepared in the same way as for the QCMs. The foil was mounted on a heating block cooled by liquid nitrogen. Mass spectra were recorded using a Balzers QMG 422 quadrupole mass spectrometer.

Extended X-ray absorption fine structure (EXAFS) spectroscopy. The EXAFS measurements of pure **2** and the host–guest complex **5** were performed at the Zn K-edge at 9659 eV at the beam line X1.1 at the Hamburger Synchrotron Radiation Laboratory (HASYLAB) at DESY, Hamburg at 20 °C with a Si (311) double crystal monochromator under ambient conditions (5.46 GeV, beam current 94 mA). Data were collected in transmission mode with ion chambers. Energy calibration was monitored with 20 μm thick zinc metal foil at a K-edge of 9659 eV. All measurements were performed under an inert gas atmosphere. The samples were prepared as a pellet of a mixture of pure **2** with polyethylene. The host–guest complex **5** was made by treating the pure **2** complex with *n*-butylamine. Data were analysed with a program package especially developed for the requirements of amorphous samples.[34] The program AUTOBK of the University of Washington[35] was used for the removal of background and the program EXCURV92[36] for the evaluation of the XAFS function. The resulting EXAFS function was weighted with k^3. Data analysis in k space was performed according to the curved-wave multiple scattering formalism of the program EXCURV92. The mean free path of the scattered electrons was calculated from the imaginary part of the potential (VPI was set to −4.00), the amplitude reduction factor AFAC was fixed at 0.8 and an overall energy shift ΔE_0 was introduced to give a best fit to the data. In the fitting procedure the coordination numbers were at first fixed to the known values for the ligands around the zinc atom in the pure **2** and the host–guest complex **5**, and after a first iteration of the bond distances and "Debye–Waller" factors varied.

3 Results and discussion

3.1 Isotherms for the sorption of amines

To characterize the sorption of volatile amines isotherms were recorded using the QCM technique. The measurements were performed by alternating the exposure of the sensors to the test gases and synthetic air. Due to requirements of fast and complete reversibility, only compounds **1**, **3** or **4** bearing sidechains with 6 or more carbon units and showing fast signals could be evaluated.

The t_{90} times of the sensors for the response to the amines were below 6 minutes and were in the same range as for other

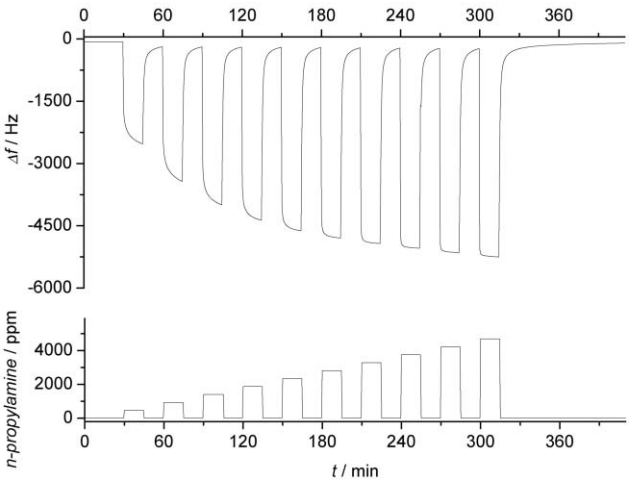

Fig. 4 Response curves of a QCM sensor coated with **4** to exposure to various concentrations of *n*-propylamine (308 K).

various VOCs (*n*-octane, toluene, acetonitrile). A typical example of 15 minute intervals for **4** are shown in Fig. 4. The response times found at low concentrations are slightly slower. This effect however is interpreted as a chromatographic effect caused by adsorption of the amines on the tubing walls.

Regarding the t_{90} recovery times, same times as for the enrichment phase were observed. For *n*-butylamine, however, the t_{90} recovery time increased and took about 16 minutes. Towards temperatures lower than 308 K even longer recovery times were observed. In these cases purging times were lengthened until complete recovery of the signal was attained. Evaluation of the isotherms for *n*-propyl- and *n*-butylamine on the PcMs was carried out and compared with the isotherms involving polyetherurethane (PEUT) which is a widely used material for QCM coatings. For comparison the isotherms for *n*-butylamine on all sensing layers are depicted in one diagram (Fig. 5).

For the metal-free **1** and the PEUT signals only reached values smaller than 500 Hz. Very large signals were however obtained for **3** and **4** already at low concentrations of amine, indicating a high affinity of the amines for zinc atoms. Compound **3**, which has more zinc atoms per gram, showed higher signals at high concentrations than **4**. A curve fit using the dual sorption mode of Henry and Langmuir sorption as presented in

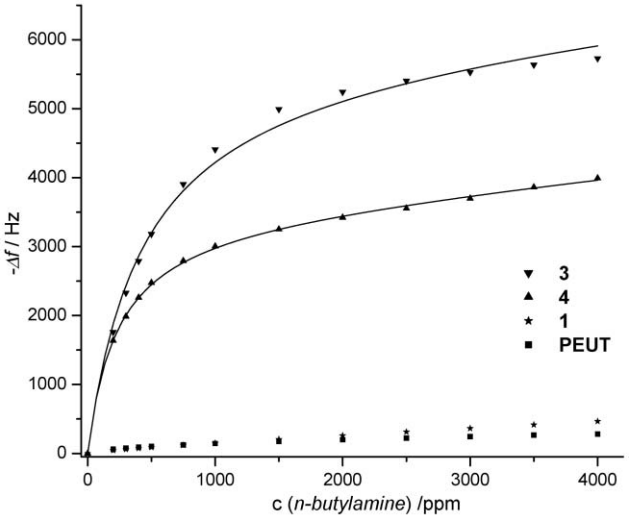

Fig. 5 Experimental isotherms for sorption of *n*-butylamine into phthalocyanine–zinc compounds **3** and **4** and into metal-free phthalocyanine **1** and reference polymer (PEUT) at 308 K. The curves for compounds **3** and **4** are obtained by curve fitting assuming a Langmuir–Henry sorption.

Table 1 Curve parameters for describing the sorptions of *n*-butylamine on different coatings

	K_{Henry}/Hz per ppm	$K_{Langmuir}$ (1/ppm)	A/Hz	$x_{stoichiometric}$
PEUT	0.11	—	—	—
1	0.09	—	—	—
3	0.12	0.0021	6000	0.99
4	0.17	0.0044	3400	0.73

Table 2 Curve parameters for describing the sorptions of *n*-propylamine on different coatings

	K_{Henry}/Hz per ppm	$K_{Langmuir}$ (1/ppm)	A/Hz	$x_{stoichiometric}$
PEUT	0.017	—	—	—
1	0.016	—	—	—
3	0.012	0.00027	5300	1.09
4	0.018	0.00068	3200	0.84

section 1 was carried out. This fit especially helps to separate the preferential Langmuir coordination from the nonpreferential sorption. The parameters obtained from the curves are listed in Table 1 and Table 2. It has to be mentioned that *n*-butylamine has a lower volatility than *n*-propylamine and hence has greater values for the binding constants K_{Henry} and $K_{Langmuir}$.

Regarding the nonspecific sorption, the K_{Henry} values are in the same order for all coatings. This indicates the same nature of nonspecific interaction for all coatings applied. In view of the selective Lewis base interaction the total amount of preferentially sorbed amine is given by the constant A. The values for *n*-butylamine are slightly larger due to its higher mass. As indicated by $x_{stoichiometric}$ all zinc sites in **3** are occupied, taking into account experimental errors. The values for phthalocyanine **4** amount to 84 and 73%. The values for the $K_{Langmuir}$ constants indicate that the zinc atoms are already coordinated at low concentrations. The concentration at which half of the metal atoms are coordinated is given by the reciprocal of $K_{Langmuir}$. According to this half the metal atoms of **4** are coordinated with about 500 ppm of *n*-butylamine and with 3700 ppm for *n*-propylamine. For **3** half of the metal atoms are coordinated at 230 ppm and at 1500 ppm, respectively.

The enthalpy of the Langmuir process was determined by performing temperature dependent measurements. Therefore the ln $K_{Langmuir}$ values were plotted *versus* the reciprocal temperature of the measurement in the so called van't Hoff plot. The values for the sorption of *n*-butylamine on **3** are depicted in Fig. 6. The values obtained for three individual sensors are in good agreement and demonstrate good experimental replication.

By linear regression the slope was determined to be 9050 $\pm$ 340 K. The value for sorption enthalpy is obtained by multiplying the slope by the gas constant R. The obtained value of $\Delta H_{Sorption} = -75$ kJ mol^{-1} is in the range of strong physisorption and hence much stronger than the condensation enthalpy of *n*-butylamine of -37 kJ mol^{-1}.

3.2 Thermal desorption mass spectrometry (TDS)

Strong evidence for the existence of two different sorption mechanisms of *n*-butylamine on the investigated phthalocyaninatozinc complexes is obtained by thermal desorption mass spectrometry (TDS). This technique was applied in order to study the kinetic characteristic of the desorption process. Therefore a substrate coated with compound **3** was placed in an UHV chamber, cooled down to the temperature of liquid nitrogen and then exposed to vapor of *n*-butylamine. Exposure for varying time duration resulted in values between 0.7 and 39 langmuir (L). The amine was subsequently desorbed by heating at a controlled rate of 1 K s^{-1} and the desorption rate was measured by using mass spectrometry. The temperature at which the maximum in the desorption rate is reached was used as a key value for the further discussion.

In Fig. 7 the temperature for the desorption maximum is plotted *versus* the coverage with *n*-butylamine. As can be seen from this plot a different behaviour is observed for high and low coverage: in the region below 4 L the temperature of the desorption maximum remains constant. This finding is typical for a first order desorption suggesting a desorption of the amine functional groups from the metal atoms which is the main form of absorbed amine at small coverage.

At values higher than 4 L a constant increase in the maximum desorption temperature is found. This finding is typical for zero order desorption like for condensates. In this case it may be interpreted by a desorption of the amine from the areas of aliphatic side chains.

3.3 Structure of pure 2 and intercalation complex 5

The experimentally determined and fitted EXAFS-function of the pure **2** and the host–guest complex **5** are shown in *k*-space as well as Fourier transforms in real space (see Fig. 8 for pure **2** and Fig. 9 for host–guest complex **5**). The structural parameters are summarized in Table 3.

The analysis of the data shows the contribution of the

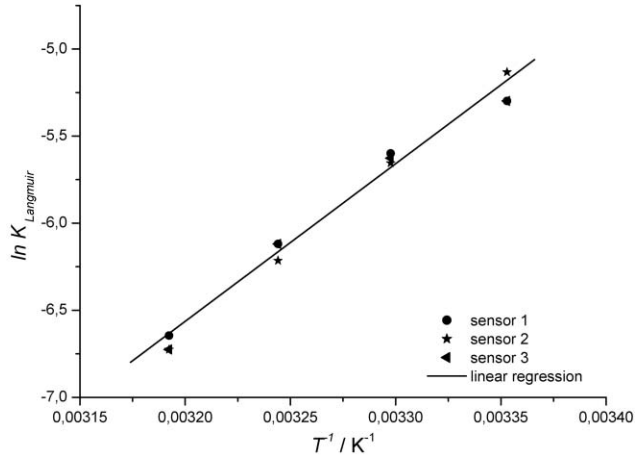

Fig. 6 Van't Hoff plot for the determination of the intercalation enthalpy of *n*-butylamine on **3**.

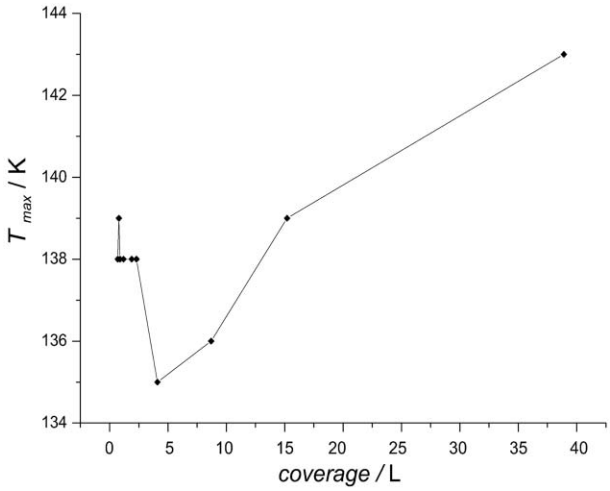

Fig. 7 Temperature of the desorption maximum of *n*-butylamine on **3** *versus* surface coverage.

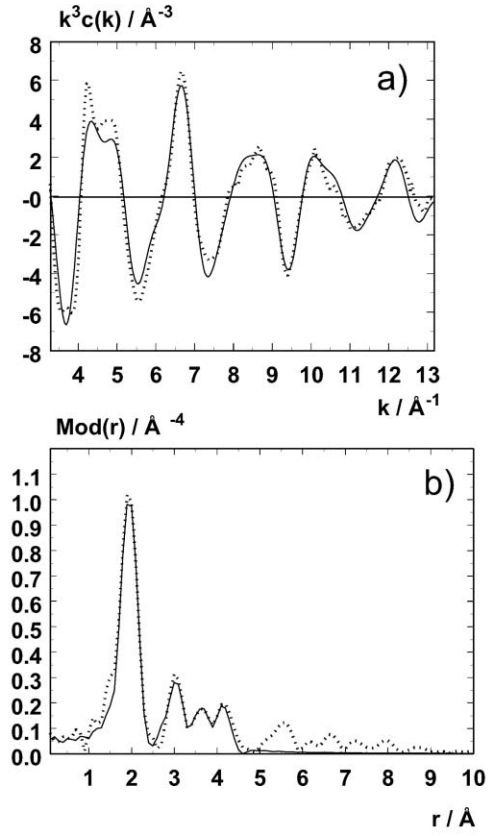

Fig. 8 Experimental (dotted line) and calculated (solid line) $k^3\chi$ (k) functions (a) (k range: 3.20–13.20 $Å^{-1}$; fit-index: 22.40; E_0: 14.15 eV) and their Fourier transforms (b) for the pure **2** (Zn K-edge; see Table 3 for fit parameter).

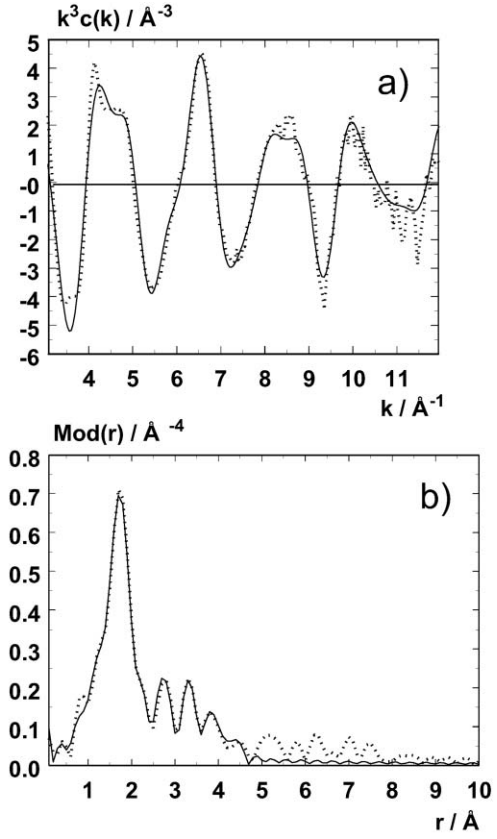

Fig. 9 Experimental (dotted line) and calculated (solid line) $k^3\chi$ (k) functions (a) (k range: 3.10–12.00 $Å^{-1}$; fit-index: 24.40; E_0: 14.09 eV) and their Fourier transforms (b) for host–guest complex **5** (Zn K-edge; see Table 3 for fit parameter).

phthalocyanine macrocycle in all spectra. About eight zinc–nitrogen distances were found in the case of both complexes, four equivalent atomic distances at about 2.00 Å, as well as four equivalent atomic distances at about 3.30 Å, respectively. Another scatterer, consisting of sixteen carbon atoms, in the case of both complexes with eight equivalent zinc–carbon distances at about 3.00 Å, as well as eight equivalent zinc–carbon distances at about 3.80 Å, was found in agreement with the well known structure of phthalocyanine, respectively. All these distances can be assigned to intramolecular contributions. The values for these distances are in good agreement with the crystallographic data[37,38] of similar compounds. In all cases the fit is significantly improved by including a Zn–Zn distance with a coordination number of two, and a Zn–(N_1') distance with a coordination number of four. Since an intermolecular Zn–(Zn′) distance was found it can be deduced that the phthalocyanine molecules are arranged in stacks. From the determined distances and the intramolecular Zn–(N_1) distance the relative orientation of the neighbouring molecules can be calculated. In the case of both complexes the molecular planes are shown to be tilted with respect to the axis connecting the centre of the molecules by a tilting angle of *ca.* 26°. In order to check this result the shortest intermolecular Zn–(N_1') distance was calculated. This distance amounts to 4.44 Å for a parallel arrangement of the molecular planes with perpendicular orientation to the axis connecting the molecular centres. In comparison to the determined distance at about 3.55 Å for both complexes, this separation is beyond the recorded EXAFS-range. (For diagrammatic representation of the tilting angle η see Fig. 10a).

When pure complex **2** is treated with *n*-butylamine, a Zn–(N_{Amin}) distance was found. This distance is already visible in the Fourier transform of the EXAFS-spectra as a shoulder in the range between 1.5 and 2.5 Å for the host–guest complex **5** (see Fig. 9b). The analysis of the spectra indicates two equivalent Zn–(N_{Amin}) distances of 2.24 Å in the case of the host–guest complex **5**. This corresponds to a 1 : 1 stoichiometry as predicted by the QCM measurements and an intercalation of *n*-butylamine between two zinc–phthalocyanine molecular planes.

For the host–guest complex **5** an intercalation of the amine group can be realised either by sp^2-hybridization of the nitrogen atom of the amine function in a planar arrangement, or by sp^3-hybridization in a tetrahedral arrangement. The nitrogen atom of the amine function is located at a distance of 1.01 Å from the zinc–zinc central axis. Due to the close position of the amine with respect to the zinc atom an orientated Lewis base coordination is suggested. This interaction is supposed to be the driving force for intercalation. No final statement can be made regarding a possible change in the hybridization of the nitrogen as *e.g.* found in tertiary aminosilanes.[39] However, sp^2-hybridization of the nitrogen in a planar arrangement does appear unlikely due to the fact that the amino function is not located in the axis of the PcM stack.

If we assume a rigid phthalocyanine molecule which is not deformed by the metal atom the shortest distance to nitrogen is 1.97 Å $\pm$ 0.02 Å.[38,40,41] Zinc–nitrogen distances of 1.98 Å in the case of the pure complex **2** and 2.00 Å in the case of the host–guest complex **5** were found. It has to be concluded that the zinc atom is located in the plane of the phthalocyanine macrocycle of both complexes (see Fig. 10).

3.4 Additional QCM measurements: exclusion of sterically demanding amines

Sterically demanding guest molecules are expected to be excluded from docking inside the phthalocyanine stacks because they have to expand the columnar arrangement of the PcMs. Therefore, the QCM sensor signals of amines of different steric demand were measured and again compared to

Table 3 EXAFS-determined structural data and structure of pure **2** and the host–guest complex **5**[a]

	Pure **2**			Host–guest complex **5**		
	N	*r*/Å	*σ*/Å	*N*	*r*/Å	*σ*/Å
Zn–(N_1)	4.4 ± 0.7	1.98 ± 0.02	0.071 ± 0.011	4.0 ± 0.6	2.00 ± 0.02	0.067 ± 0.013
Zn–(N_{Amin})	—	—	—	**1.8 ± 0.3**	**2.24 ± 0.02**	**0.126 ± 0.019**
Zn–(C_2)	8.0 ± 1.2	2.99 ± 0.03	0.122 ± 0.025	8.0 ± 1.2	3.07 ± 0.03	0.100 ± 0.030
Zn–(N_3)	4.0 ± 0.6	3.31 ± 0.03	0.074 ± 0.012	4.0 ± 0.6	3.33 ± 0.03	0.050 ± 0.008
Zn–(C_4)	8.1 ± 1.2	3.78 ± 0.04	0.074 ± 0.015	8.1 ± 1.2	3.83 ± 0.04	0.074 ± 0.022
Zn–(Zn′)	2.2 ± 0.3	3.94 ± 0.04	0.094 ± 0.010	2.3 ± 0.3	4.00 ± 0.04	0.089 ± 0.018
Zn–(N_1′)	4.2 ± 0.6	3.56 ± 0.04	0.102 ± 0.015	4.0 ± 0.6	3.55 ± 0.04	0.110 ± 0.022
η/°	26.2 ± 2.0			27.5 ± 2.0		

[a]Coordination number *N*, absorber–backscatterer distance *r* and Debye–Waller factor *σ* with calculated standard deviations and the tilting angle *η*. The letters in parentheses refer to the pure **2** and the host–guest complex **5** in Fig. 10 and indicate the molecule where the back-scattering atom is located.

PEUT. To compensate for the different volatility of the amines the concentration units are given as partial pressure *p* divided by the saturation pressure p° at the measurement temperature.

Significantly smaller sensor signals of the branched 2-butylamine and *tert*-butylamine were observed as compared with the linear *n*-butylamine. As can be seen in Fig. 11 the calibration curves recorded for the *tert*-butylamine only show signals of about 60% compared with the linear n-butylamine. Signals for the branched 2-butylamine are in between. The most sterically demanding *tert*-butylamine is less strongly enriched. The enrichment in the nonspecific PEUT layer is smaller by a factor of 10 and does not differentiate between the amines offered. However, a complete exclusion of *tert*-butylamine from the docking places is not found.

A model showing an idealized intercalation visualizes the extent of exclusion (*cf.* Fig. 12). As a basis the structural data determined by EXAFS (intermolecular distance of 4.00 Å, Zn–(N-amine)-distance of 2.24 Å) were used. As can be seen from the illustration in Fig. 12, an intercalation of linear molecules is possible. For *tert*-butylamine an approach of the amine function to the zinc atom, however, is only possible up to a distance of approximately 4 Å. With further approach the van der Waals radii of the amine and the PcM basic structure would overlap significantly. Following these considerations, reasons for the smaller sensor signals might result from an energetically unfavored widening of the PcZn staples and consequent smaller intercalation enthalpies.

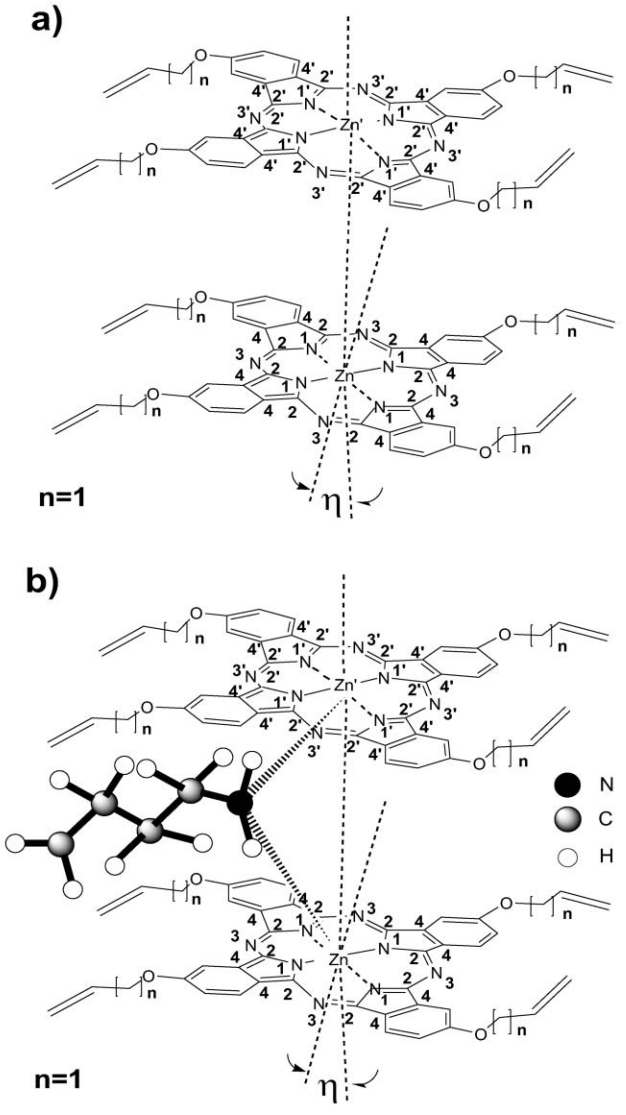

Fig. 10 Proposed structure of the pure **2** (a), and of the host–guest complex **5** (b) with intercalated *n*-butylamine, tilting angle *η* and chain length *n* = 1.

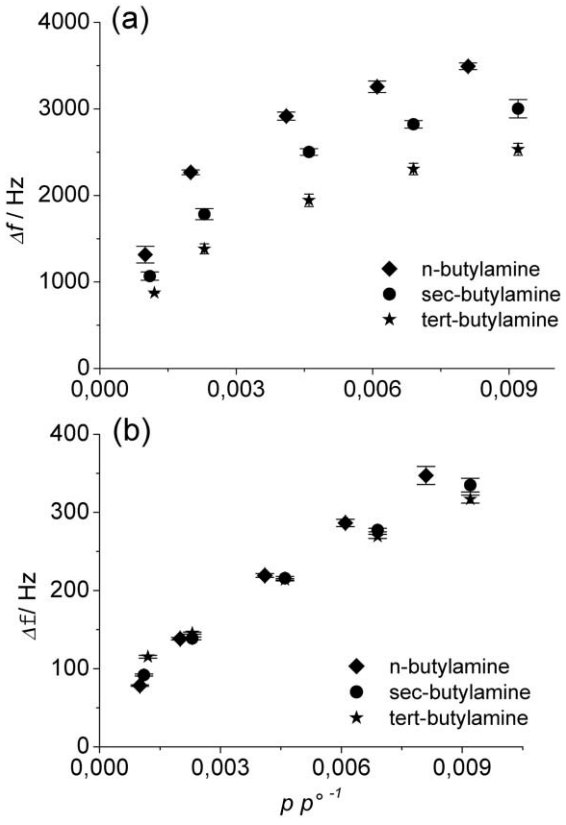

Fig. 11 Experimental sensor calibration curves for the enrichment of different sterically demanding amine molecules: (a) for phthalocyanine **3** and (b) for PEUT.

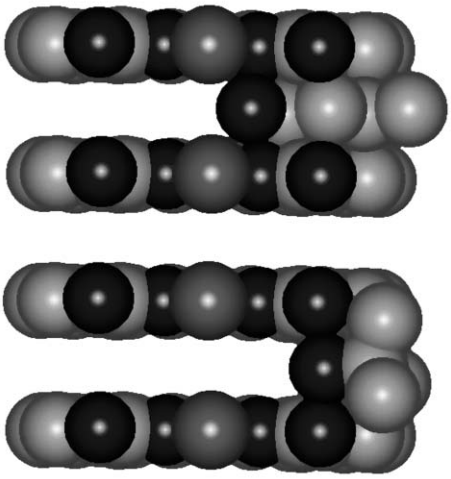

Fig. 12 Side view of intercalated *n*-butylamine (above) and *tert*-butylamine (below) between stacks of PcZn. For reasons of simplicity side groups and hydrogen atoms are omitted.

4 Conclusions

The coexistence of two different sorption behaviors of amines into the columnar structure of 2,9,16,23-tetrakis(alkenyloxy)-phthalocyaninatozinc could be shown by QCM and TDS measurements. The sorption process can be described by a superposition of nonpreferential Henry-type and preferential Langmuir-type sorption. The binding enthalpy for *n*-butylamine on 2,9,16,23-tetrakis(hex-5-enyloxy)phthalocyaninatozinc was determined by temperature dependent QCM measurements to be -75 kJ mol^{-1} for the Lewis base coordination. For the QCM sensor applications this bulk effect is important, as it allows working with large layer thicknesses and leads to improved sensitivity.

The EXAFS measurements for the exposure of *n*-butylamine to pure 2,9,16,23-tetrakis(prop-2-enyloxy)phthalocyaninatozinc provided the following geometric parameters: The nitrogen of the amino group is located at a distance of 2.24 Å to the zinc atoms and 1.01 Å from the stack axis. The columnar arrangement of the phthalocyanine does not change significantly during the amine uptake. This finding is explained by intercalation of the amine.

Investigation of sterically demanding amines showed that the linear *n*-butylamine is favorably sorbed by the phthalocyanine coating. Consequently the coatings can be used to enhance selectivity in chemical sensing applications in contrast to statistically ordered soft polymers, and in addition to improve the functional selectivity caused by the metal–amine interaction.

Acknowledgement

We gratefully acknowledge the funding provided by the Deutsche Forschungsgemeinschaft (DFG) within the framework of the research group "Molecular pattern recognition using supramolecular compounds and polymers" (FKZ Go 301/23-3) and the DFG Graduiertenkolleg "Chemistry in interphases". The research group at the Department of Physical Chemistry would not have been possible without the knowledge and enthusiasm of W. Göpel.

We also thank T. Weiβ and M. Wandel for their assistance in performing the TDS measurements.

References

1 A. Hierlemann, A. J. Ricco, K. Bodenhöfer, A. Dominik and W. Göpel, *Anal. Chem.*, 2000, **72**, 3696–3708.
2 U. Weimar and W. Göpel, *Sens. Actuators B*, 1998, **52**, 143–162.
3 J. W. Grate, *Chem Rev.*, 2000, **100**, 2627–2648.
4 P. C. Jurs, G. A. Bakken and H. E. McClelland, *Chem. Rev.*, 2000, **100**, 2649–2678.
5 J. Park, W. A. Groves and E. T. Zellers, *Anal. Chem.*, 1999, **71**, 3877–3886.
6 C. Fietzek, K. Bodenhöfer, P. Haisch, M. Hees, M. Hanack, S. Steinbrecher, F. Zhou, E. Plies and W. Göpel, *Sens. Actuators B*, 1999, **57**, 88–98.
7 H. O. Finklea, M. A. Phillippi, E. Lompert and J. W. Grate, *Anal. Chem.*, 1998, **70**, 1268–1276.
8 A. Hierlemann, K. Bodenhöfer, M. Fluck, V. Schurig and W. Göpel, *Anal. Chim. Acta*, 1997, **346**, 327–339.
9 A. Battenberg, V. F. Breidt and H. Vahrenkamp, *Sens. Actuators B*, 1996, **30**, 29–34.
10 R. Paolesse, C. DiNatale, V. Campo Dall'Orto, A. Macagnano, A. Angelaccio, N. Motta, A. Sgarlata, J. Hurst, I. Rezzano, M. Mascini and A. D'Amico, *Thin Solid Films*, 1999, **354**, 245–250.
11 F. L. Dickert, G. Bertlein, G. Mages and W.-E. Bulst, *Adv. Mater.*, 1990, **2**, 420–422.
12 J. W. Grate, S. J. Patrash and S. N. Kaganove, *Anal. Chem.*, 2000, **71**, 1033–1040.
13 K. Bodenhöfer, A. Hierlemann, M. Juza, V. Schurig and W. Göpel, *Anal. Chem.*, 1997, **69**, 4017–4031.
14 F. L. Dickert, A. Haunschild, V. Kuschow, M. Reif and H. Stathopulos, *Anal. Chem.*, 1996, **68**, 1058–1061.
15 D. Kriz, O. Ramström and K. Mosbach, *Anal. Chem.*, 1997, 345A–349A.
16 R. Buchhold, A. Nakladal, G. Gerlach, M. Herold, G. Gauglitz, K. Sahre and K.-J. Eichhorn, *Thin Solid Films*, 1999, **350**, 178–185.
17 B. Kieser, D. Pauluth and G. Gauglitz, *Anal. Chim. Acta*, 2001, **434**, 231–237.
18 J. Brettar, J.-P. Gisselbrecht, M. Gross and N. Solladié, *Chem. Commun.*, 2001, 733–734.
19 N. A. Rakow and K. S. Suslick, *Nature*, 2000, **406**, 710–713.
20 C. S. Giam, J. Itoh and J. E. Leonard, *Int. J. Environ. Anal. Chem.*, 1984, **16**, 285–293.
21 A. Hierlemann, A. J. Ricco, K. Bodenhöfer and W. Göpel, *Anal. Chem.*, 1999, **71**, 3022–3035.
22 C. F. van Nostrum and R. J. M. Nolte, *Chem. Commun.*, 1996, **21**, 2385–2392.
23 B. M. Hassan, H. Li and N. B. McKeown, *J. Mater. Chem.*, 2000, **10**, 39–45.
24 B. Görlach, PhD thesis, University of Tübingen, 2000.
25 E. A. Stern, *Phys. Rev. B*, 1974, **10**, 3027.
26 F. W. Lytle, D. E. Sayers and E. A. Stern, *Phys. Rev. B*, 1975, **11**, 4825.
27 G. Sauerbrey, *Z. Phys.*, 1959, **155**, 206.
28 J. W. Grate, S. J. Martin and M. W. White, *Anal. Chem.*, 1993, **65**, 987A.
29 K. Bodenhöfer, A. Hierlemann, M. Juza, V. Schurig and W. Göpel, *Anal. Chem.*, 1997, **69**, 4017–4031.
30 A. Michalke, A. Janshoff, C. Steinem, C. Henke, M. Sieber and H.-J. Galla, *Anal. Chem.*, 1999, **71**, 2528–2533.
31 B. Görlach, M. Dachtler, T. Glaser, K. Albert and M. Hanack, *Chem. Eur. J.*, 2001, **7, No. 11**, 2459.
32 S. Steinbrecher, F. Zhou, E. Plies and M. Hanack, *J Porphyrins Phthalocyanins*, 2000, **4**, 10–18.
33 K. Bodenhöfer, A. Hierlemann, R. Schlunk and W. Göpel, *Sens. Actuators B*, 1997, **45**, 259–264.
34 T. S. Ertel, H. Bertagnolli, S. Hückmann, U. Kolb and D. Peter, *Appl. Spectrosc.*, 1992, **46**, 690.
35 M. Newville, P. Livins, Y. Yakobi, J. J. Rehr and E. A. Stern, *Phys. Rev. B*, 1993, **47**, 14126.
36 S. J. Gurman, N. Binsted and I. Ross, *J. Phys. C*, 1986, **19**, 1845.
37 L. H. Vogt Jr., A. Zalkin and D. H. Templeton, *Inorg. Chem.*, 1967, **6**, 1725.
38 J. S. Miller, C. Vazquez, J. C. Calabrese, R. S. McLean and A. Epstein, *Adv. Mater.*, 1994, **6**, 217.
39 H. Fleischer, P. T. Brain, D. W. H. Rankin, H. E. Robertson, M. Bühl and W. Thiel, *J. Chem. Soc., Dalton Trans.*, 1998, 593–600.
40 L. H. Vogt Jr., A. Zalkin and D. H. Templeton, *Inorg. Chem.*, 1967, **6**, 1725.
41 D. Wöhrle and G. Mayer, *Kontakte (Darmstadt)*, 1985, **3**, 38.